

Self-consistent petrological-thermomechanical modelling: new geodynamic modelling approach.

Taras V. Gerya^a, James A.D. Connolly^a, David A. Yuen^b

^a Department of Earth Sciences, Swiss Federal Institute of Technology (ETH - Zürich),
Sonneggstrasse 5, CH-8092 Zurich, Switzerland

^c University of Minnesota Supercomputing Institute *and* Department of Geology and
Geophysics, University of Minnesota, Minneapolis, 117 Pleasant St. SE Minnesota 55455-
0219, USA, davey@krissy.geo.umn.edu

We have developed a coupled petrological-thermomechanical modeling approach to investigate the dynamical effects of phase transformations (including melting) on various geodynamic processes. We have included density changes due to phase transitions in both the continuity and the momentum equations, and latent heat of mineral reactions and adiabatic and shear heating in the energy conservation equation. The continuity equation is solved in Lagrangian form with substantive time derivative of density computed from moving active markers. The model rheology is viscoelastoplastic and dependent on pressure, temperature, stresses and strain rate as well as chemical and mineralogical composition. The petrological model covers both crustal rocks and the mantle and is derived by free energy minimization together with estimates for the thermodynamic properties of crustal and mantle minerals. This approach precisely quantifies the thermodynamic and mechanical influence of phase transformations, which depend on temperature, pressure and composition. We have applied a well-tested marker-in-cell method and conservative finite-differences to solve governing equations in 2-D. Our highest-resolution simulations to date use 40 billion markers. This extremely high resolution results in uncompressed output file sizes of 840 GB or more for each time step. Similar amounts of memory are required during runs as well, but the latest shared-memory supercomputers such as COBALT at NCSA have ample memory for these large runs. We have implemented a parallel computing with Open MP and a compressed file format for output that is capable of reducing file sizes by at least three orders of magnitude indeed allowing rerunning from the compressed output.

Example 1 (Fig. 1): We have recently used a coupled petrological-thermomechanical model to investigate the dynamical effects of metamorphic reactions and melting on the seismic structure of thermal-chemical plumes beneath volcanic arcs. Plume generation is driven by the subduction of buoyant crustal rocks and expulsion of aqueous slab fluids that causes hydration and partial melting of the mantle wedge. The model demonstrates two chemically distinct types of plumes. Unmixed plumes initiate from the melting front within the mantle that arises as a consequence of infiltration of slab-derived water-rich fluids, whereas mixed plumes initiate from the slab itself and entrain both slab and mantle derived magmas. Mixed plumes explain magmas such as adakites with crustal signatures, while primitive arc tholeiites are attributed to unmixed plumes. Our simulations also indicate that parts of the mantle wedge can become trapped between rheologically weak, hydrated, and partially molten upwellings (cold plumes) and the subducting slab. The structures form at various depths and develop circular, elliptic, or irregular shapes. The combined effect of the tractions caused by upwelling and subduction causes these regions to rotate. Our simulations investigate the parameters controlling the occurrence and long-term stability of such rigid, rotating structures. Circular rotating structures like “subduction wheels” are characteristic of models with relatively

young (20–30 Myr) slabs and intermediate (2–5 cm/yr) subduction rates. We propose that the development of such circular features may explain some of the isolated seismic velocity anomalies in the mantle wedge. As a consequence of the interplay between water content and temperature both positive and negative seismic velocity anomalies are associated with the plumes. Positive anomalies are prevalent close to the slab due to the lowered temperatures associated with regions of cold plume initiation. Negative seismic anomalies develop at shallower depth due to the partially molten rocks that form plume heads. Flat lying partially molten regions that form beneath volcanic arcs as a consequence of cold wet plumes are manifest by $> 20\%$ variations in the local Poisson ratio, as compared to variations of $\sim 2\%$ expected as a consequence of temperature variation within the mantle wedge. In contrast to models that attribute a purely thermal origin for mantle wedge seismic anomalies, the petrological-thermomechanical model is able to explain the strong seismic velocity variations existing beneath volcanic arcs.

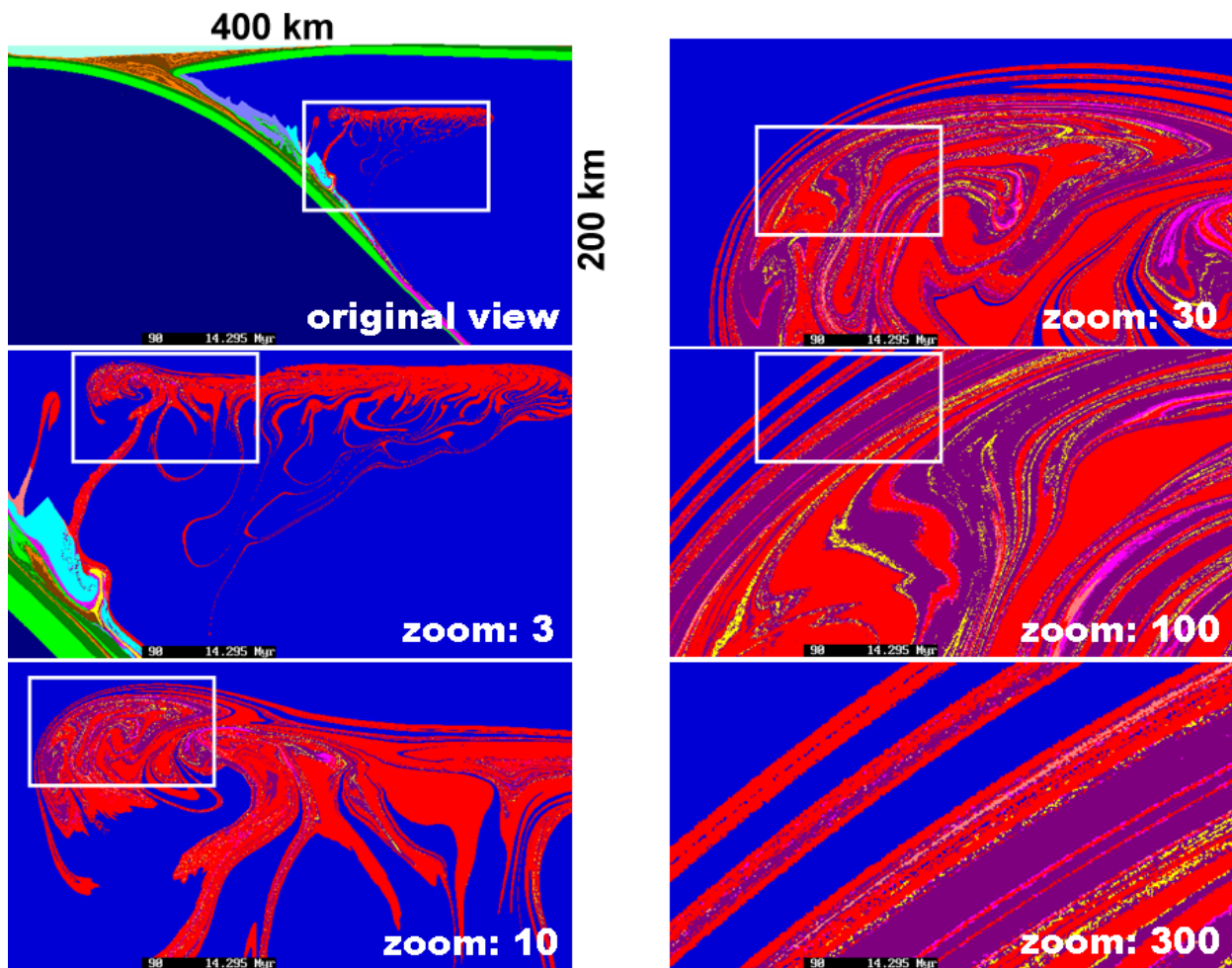


Figure 1. High resolution multiple scale visualization of mechanical stirring structures related to development of partially molten plumes (red) in subduction zone (Gerya & Yuen, 2003a; Gerya et al., 2006; Gorczyk et al., 2006). 40 billion element (pixel) data set with spatial resolution of ~ 2 m is based on compressed output from the numerical experiment with 10 billion markers.

Example 2 (Fig. 2, 3, 4): Intrusions of ultramafic bodies into the lower density crust are documented for a large variety of tectonic settings spanning continental shields, rift systems collision orogens and magmatic arcs. The intriguing point is that these intrusive bodies have a density higher by $300\text{--}500\text{ kg/m}^3$ than host rocks. This paradox requires understanding of emplacement mechanism. We carried out a 2-D simplified version of petrological-

thermomechanical modeling study of intrusion of partly crystallized ultramafic magma from sub-lithospheric depth to the crust through a pre-existing magmatic channel. Systematically varying model parameters allows documenting variations in intrusion dynamics and geometry that range from funnel- and finger-shaped bodies (pipes, dikes) to deep seated balloon-shaped intrusions and flattened shallow magmatic sills. Emplacement of ultramafic bodies in the crust lasts for several kyr to several hundreds kyr depending mainly on the viscosity of the intruding magma. The positive buoyancy of the magma compared to the overriding colder mantle lithosphere drives intrusion while the crustal rheology controls the final location and the shape of the ultramafic body. Relatively cold elasto-plastic crust ($T_{\text{Moho}}=400^{\circ}\text{C}$) promotes strong upward propagation of magma due to the significant decrease of plastic strength of the crust with decreasing confining pressure. Emplacement is in this case controlled by crustal faulting and subsequent block displacements. Warmer crust ($T_{\text{Moho}}=600^{\circ}\text{C}$) triggers lateral spreading of magma above the Moho with emplacement being accommodated by coeval viscous deformation of the lower crust and fault tectonics in the upper crust. Strong effects of magma emplacement on the surface topography are also documented. Emplacement of high density, ultramafic magma into low-density rocks is a stable mechanism for a wide range of model parameters matching geological settings in which partially molten mafic-ultramafic rocks can be formed below the lithosphere. We expect this process to be particularly active below subduction-related magmatic arcs where huge volumes of partially molten rocks produced from hydrous cold plume activity accumulate below the overriding lithosphere (Figure 1).

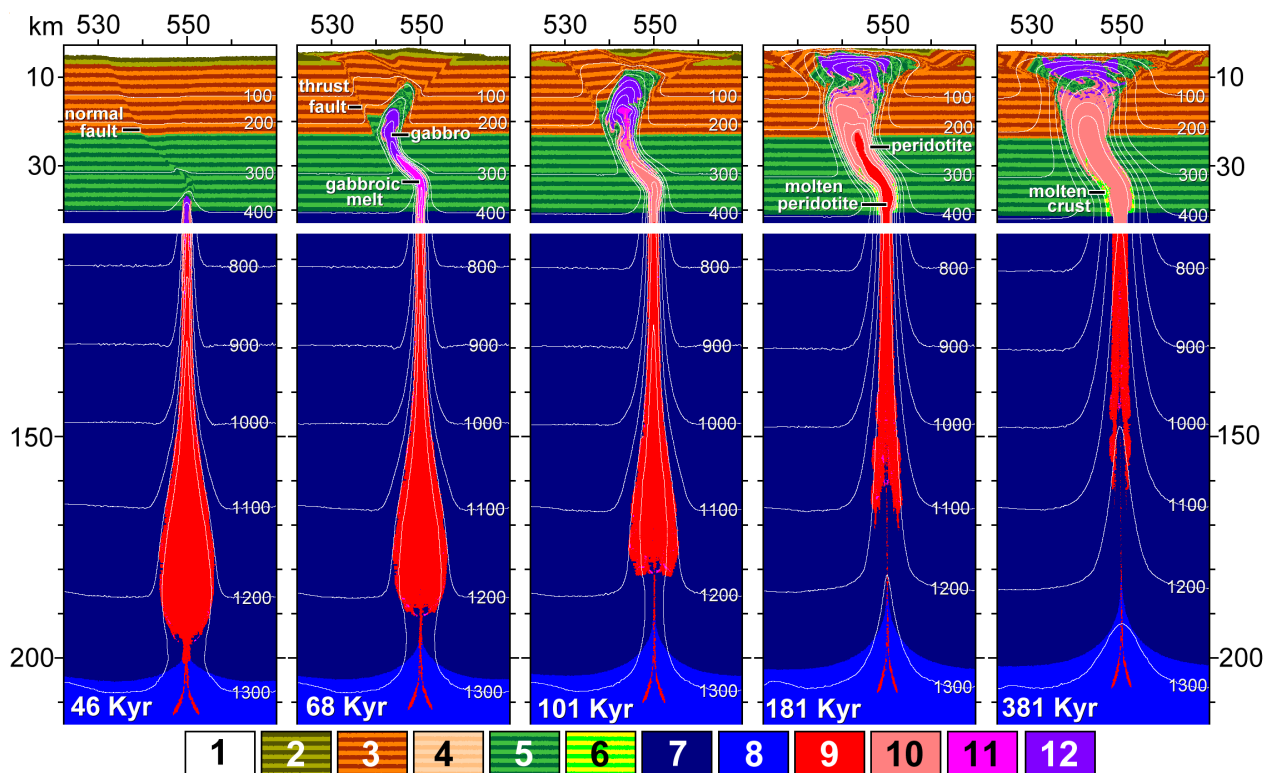


Figure 2. Enlarged 50 x 215 km areas of the original 1100 km x 300 km model. Distribution of rock layers in the intrusion area during emplacement of the ultramafic body into the crust from below the lithosphere via the magmatic channel. Color code: 1 = weak layer (air, water); 2 = sediments; 3,4 = upper crust (3 - solid, 4 - molten); 5,6 = lower crust (5 - solid, 6 - molten); 7,8 = mantle (7 - lithospheric, 8 - asthenospheric); 9,10 = peridotite (9 - molten, 10 - crystallized); 11,12 = gabbro (11 - molten, 12 - crystallized). Time (kyr) is given in the figures. White numbered lines are isotherms in $^{\circ}\text{C}$. Vertical scale: depth below the upper boundary of the model.

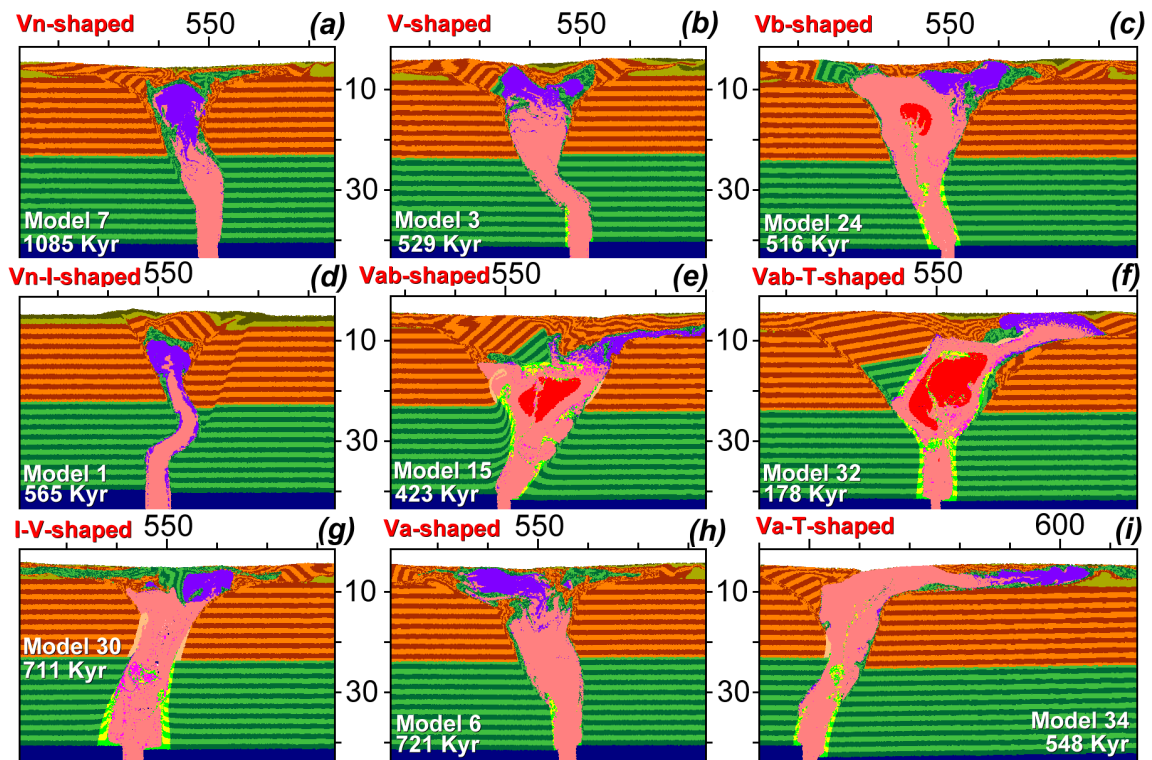


Figure 3. Major types of culminate shapes of intrusions obtained in numerical experiments due to the variations in the model parameters. Red letters denote intrusion shapes: V - funnel-shaped; I - finger-shaped; T - nappe(sill)-shaped; a - asymmetric; b - broad; n - narrow. Rock types are the same as in Figure 2.

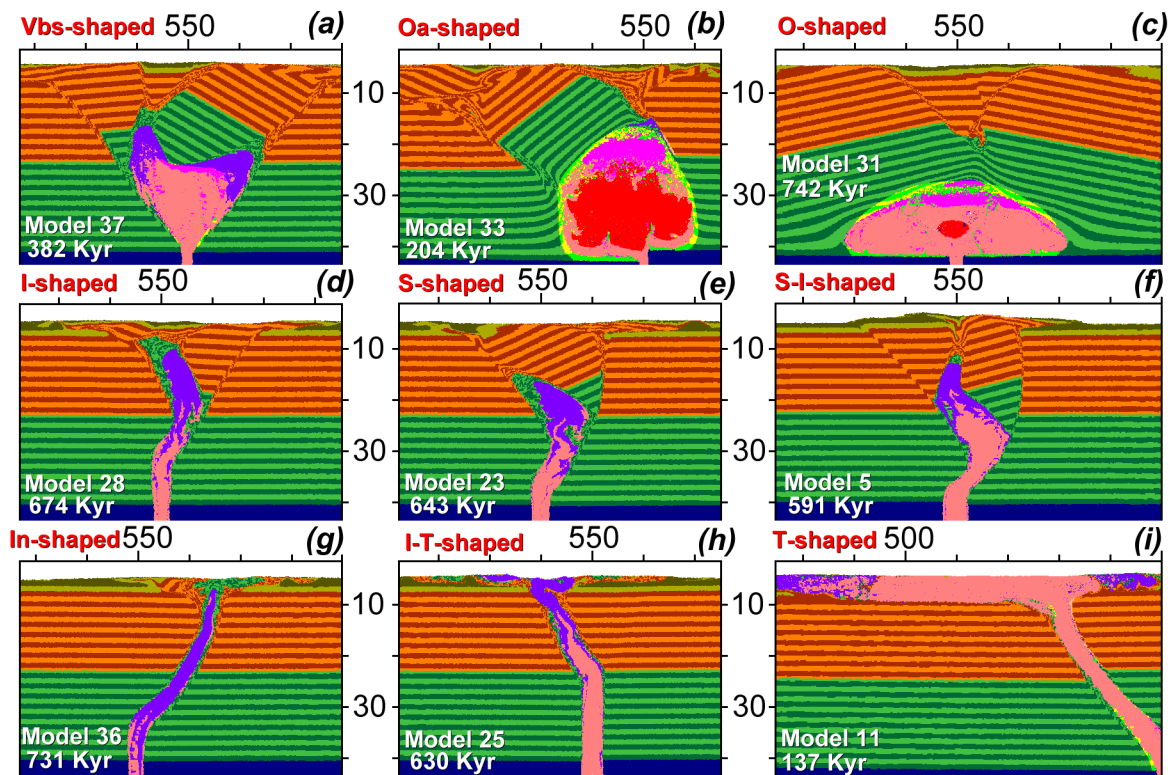


Figure 4. Major types of culminate shapes of intrusions obtained in numerical experiments due to the variations in the model parameters. Red letters denote intrusion shapes: O - balloon-shaped; V - funnel-shaped; S - sickle-shaped; I - finger-shaped; T - nappe(sills)-shaped; a - asymmetric; b - broad; n - narrow; s - short. Rock types are the same as in Figure 2.